Density reduction effects on the production of [11C]CO2 in Nb-body targets on a medical cyclotron

Mues genannt Koers, Lucas; Prevost, David; Paulssen, Elisabeth; Hoehr, Cornelia

DOI
10.1016/j.apradiso.2023.110911

Publication date
2023

Document Version
Final published version

Published in
Applied Radiation and Isotopes

Applied Radiation and Isotopes 199 (2023) 110911

Contents lists available at ScienceDirect

Applied Radiation and Isotopes

journal homepage: www.elsevier.com/locate/apradiso

Density reduction effects on the production of [11C]CO2 in Nb-body targets on a medical cyclotron

Lucas Mues genannt Koers [a,b], David Prevost [a], Elisabeth Paulssen [b,c], Cornelia Hoehr [a,*]

[a] Life Sciences Division, TRIUMF, 4004 Wesbrook Mall, Vancouver, BC, V6T 2A3, Canada
[b] Faculty of Chemistry and Biotechnology, FH Aachen, Heinrich-Mußmann-Str. 1, 52428, Jülich, Germany
[c] TU Delft, Department of Radiation Science and Technology, Mekelweg 15, 2629 JB, Delft, the Netherlands

ARTICLE INFO

Keywords:
C-11
Carbon-11
PET-Isotope
Medical cyclotron

ABSTRACT

Medical isotope production of ^{11}C is commonly performed in gaseous targets. The power deposition of the proton beam during the irradiation decreases the target density due to thermodynamic mixing and can cause an increase of penetration depth and divergence of the proton beam. In order to investigate the difference how the target-body length influences the operation conditions and the production yield, a 12 cm and a 22 cm Nb-target body containing N_2/O_2 gas were irradiated using a 13 MeV proton cyclotron. It was found that the density reduction has a large influence on the pressure rise during irradiation and the achievable radioactive yield. The saturation activity of $[^{11}C]CO_2$ for the long target (0.083 Ci/μA) is about 10% higher than in the short target geometry (0.075 Ci/μA).

1. Introduction

Carbon-11 is widely applied in positron emission tomography (PET) for numerous medical applications or life science studies. Regarding its half-life of approximately 20 min and the positron emission ratio of 99.8% (Magill et al., 2018), ^{11}C is well suited for PET studies.

^{11}C and other widely used positron emitters are produced by low energy cyclotron irradiation of gas targets. Roughly, about 1000 of these small cyclotrons are globally available (Schaffer et al., 2015) and enable convenient on-site preparation of imaging pharmaceuticals. To guarantee appropriate production of PET tracers in small cyclotrons, extensive knowledge of gas target irradiation using low energy charged particles is mandatory.

In the past years, multiple studies aimed to improve gas target radionuclide production by optimizing target geometry and reducing adsorption of radionuclides at the walls of the target (Buckley et al., 2000, 2004; Zacchia et al., 2018). These studies concluded that produced ^{11}C nuclides can stick to the target wall, reducing the achievable radioactive yield. A decrease of the adsorption of ^{11}C on the target wall was achieved by using niobium as the inert target body material (Buckley et al., 2004). Furthermore, changing the target geometry to a conical shape instead of a cylindrical shape showed a slight improvement of radioactive yield due to the adjusting of the target body to the beam broadening (Buckley et al., 2000). Similarly, Jahangiri et al. (2016) showed increased production yields using a conical shaped niobium target, justified by the superior natural convection of cylindrical shaped target geometries. This observation was further confirmed by Uittenbosch et al. (2018), investigating the influence of natural and forced convection on the production yield of gas target irradiation.

Originally, convection studies were performed addressing the density reduction in gaseous targets upon charged particle beam irradiation first observed around the 1960s and 1970s (Oselka et al., 1977; Robertson et al., 1961; McDaniels et al., 1972). Further extensive investigations on the density reduction of gas targets at impinging protons beams revealed a dependency of the penetration depth and geometry on the beam current and gravity in gaseous as well as liquid targets (Heselius et al., 1982; Heselius and Solin, 1986; Jahangiri et al., 2018) resulting in a self-sustained pressure oscillation (Jahangiri et al., 2018). This oscillation was explained due to the proton beam leaving the back of the target due to heat induced density reduction, causing less energy deposition followed by less heat transfer, resulting in a cooling of the target and an increase of density. Therefore, the proton beam was fully stopped in the target volume, starting the heating period of the gas target again.

Considering the density reduction and corresponding increase in beam penetration, the design of a “beam-thick” target, a target where

* Corresponding author.
E-mail address: choehr@triumf.ca (C. Hoehr).

https://doi.org/10.1016/j.apradiso.2023.110911
Received 6 February 2023; Received in revised form 6 June 2023; Accepted 21 June 2023
Available online 22 June 2023

the beam is fully absorbed inside the target, is desirable. High beam currents are advantageous to increase the yield, but targets that are too small to fully compensate for the density reduction might result in the beam penetration exceeding the target length and not depositing all its energy in the target, which in turn causes lower product yield.

To further investigate the extend of density reduction in gas target radio nuclide production, we studied the pressure increase and production yield for the production of ^{11}C at different target lengths. The production of ^{11}C by the $^{14}N(p,\alpha)^{11}C$ reaction was carried out in a 12 cm and a 22 cm long cylindric shaped target body, monitoring the target performance and the production yield. The pressure rise in the two targets was analyzed with our previously published model (Jahangiri et al., 2016).

2. Materials and methods

2.1. Irradiations

The influences of a long body target in comparison to a short body target were studied using TRIUMF's TR13 cyclotron (Vancouver BC, Canada, from Advanced Cyclotron Systems Inc., Richmond BC Canada). TR13 is a 13 MeV shelf-shielded negative hydrogen ion cyclotron. Protons were obtained by removing the electrons from the hydrogen ions using a thin carbon foil followed by a change of charge. The final beam was collimated to a 10 mm wide circularly Gaussian beam entering the target body. The target bodies were shielded from cyclotron vacuum using a 25 μm thick aluminum foil and a 38 μm thick HAVAR® foil (Goodfellow Corporation Corapolis, PA, USA) containing a helium cooling stream of 120 L min^{-1} between both foils. This separation set up caused a beam attenuation to 12 MeV (0.2 MeV absorption originating from the aluminum foil and 0.8 MeV from HAVAR® foil (Jahangiri et al., 2016); calculated using SRIM 2013 software (Ziegler et al., 2010) at entrance of the target. Further cooling was achieved by outside water cooling of the target bodies using a flow of 3 L/min. A schematic depicting of the applied target setups is presented in Fig. 1.

All irradiations (regardless the target size) were performed using a proton beam between 21 and 32 μA current. The starting target pressure was set to be between around 288 and 323 psi (19.9–22.3 bar) providing a sufficiently high amount of target material while leaving enough room for pressure increase. An increasing pressure, exceeding 450 psi (31 bar), entails the risk of the separation foils failing. An irradiation time of 24–36 min was chosen. A summary of the irradiation parameters is presented in Table 1.

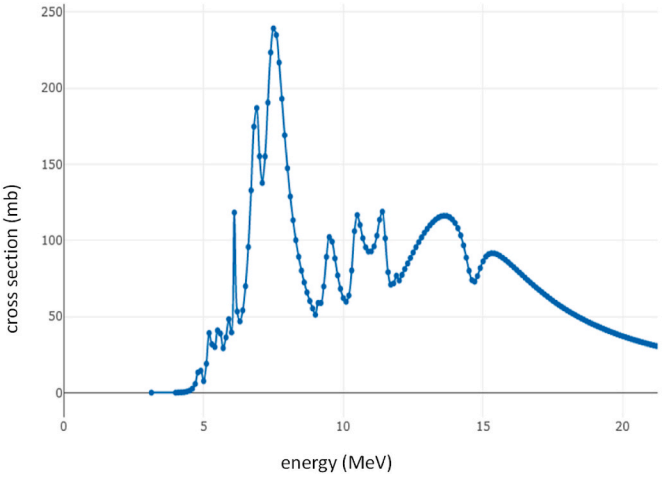

Fig. 2. Production cross section for $^{14}N(p,\alpha)^{11}C$. Data from (IAEA, 2022).

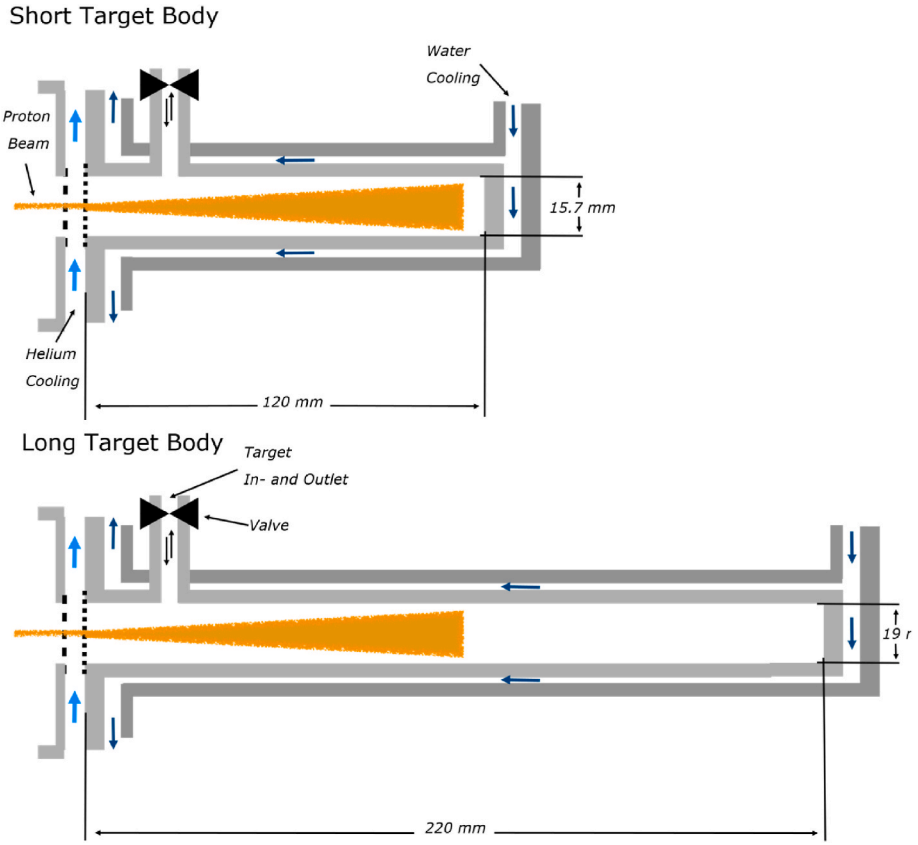

Fig. 1. Schematic of the short (top) and long (bottom) target body with the proton beam in orange. The light blue arrows depict the He flow across the two entrance foils for cooling, while the dark blue arrows indicate the water-cooling flow over the target body.

Table 1
Beam current I, initial target pressure p_0 and irradiation time t for the short and long target irradiation. The yield was measured in the short target for S1, S2, and S4, and in the long target for L1, L3, and L4. The error on the pressure is ±0.5 psi and the error on the time is ±0.5 min.

Run	Target	I (μA)	p_0 (psi)	t (min)
S1	Short	23.6 ± 0.4	323	32
S2	Short	24.9 ± 0.4	314	30
S3	Short	29.2 ± 0.5	312	31
S4	Short	30.0 ± 0.5	312	30
L1	Long	20.9 ± 0.3	319	36
L2	Long	25.5 ± 0.4	295	31
L3	Long	26.4 ± 0.4	288	30
L4	Long	31.5 ± 0.7	289	24

2.2. Targets

2.3 Two target bodies were constructed out of Nb with different lengths and diameters, see Fig. 2. Both target bodies have a flange which allows the target to be mounted onto the cyclotron onto a helium cooling window. The targets each have a connection to the product gas line functioning as in- and outlet to load and unload the target remotely with the target gas mixture. Both have an aluminium jacket around the target body with water inlet and outlet to provide water colling during irradiation. The only difference between the two designs is the size of the gas chamber. The short target has an inner gas chamber length of 120 mm and an inner diameter of 15.7 mm. The long target has an inner gas chamber length of 220 mm and an inner diameter of 19.0 mm. These dimensions were chosen, as a SRIM simulation (Ziegler et al., 2010) of 13 MeV protons impinging into the target gas with a typical loading pressure of 312 psi showed a maximum proton range of 80 mm. This means that any difference in yield between the short and long target is likely due to density reduction and thermodynamic effects.*Pressure rise measurement*

The pressure p in the two targets during irradiations was measured after tuning the beam and compared to the initial loading pressure p_0. It was then analyzed with our previously published model (Jahangiri et al., 2016). In summary, the target reaches thermal equilibrium very shortly after the start of the irradiation and the beam power deposition $S = \Delta T \bullet H$ is a product of the temperature rise ΔT above the initial temperature T_0, and the overall heat removal H, which is defined based on the overall heat transfer coefficient h of the target chamber system and the contact area A, with $H = h \bullet A$.

Together with the ideal gas law $= n \bullet R \bullet T/V$, with n the number of moles of the gas, T the temperature of the target, R the Avogadro constant, and V the volume of the target, and a linear expansion of the heat transfer coefficient $h = h_0 + h_1 \bullet S/S_m$ with S_m the maximum beam deposition, we found that the pressure rise can be approximated as (see (Jahangiri et al., 2016) for the details of the derivation):

$$\frac{p}{p_0} = 1 + \frac{S}{\left(h_0 + h_1 \bullet \frac{S}{S_m}\right) \bullet A \bullet T_0} \quad (1)$$

This is consistent with the empirical solution $\frac{p}{p_0} = 1 + a \bullet I^b$ by (Wojciechowski et al., 1988) with a and b being fitting parameters. Eq. (1) gives a more physical meaning to the fitting parameters h_0 and h_1. As without beam present, h reduces to h_0, this can be interpreted as the heat transfer coefficient only dependent on geometry and material considerations. In contrast, h_1 is dependent on the beam power and the target temperature rise. A large h_1 can be interpreted as a large amount of heat removal due to strong convective currents being formed in the target during irradiation.

2.3. Activity measurement

For the production of ^{11}C, natural N_2 gas, containing mostly ^{14}N isotopes (99.64%) (Magill et al., 2018), was irradiated resulting in almost exclusively $^{14}N(p,\alpha)^{11}C$ reactions. The cross sections for this reaction are presented in Fig. 2. Additionally, 0.5% O_2 gas (Zacchia et al., 2018; Jahangiri et al., 2016) was added to the N_2 target gas, to enable the formation of $^{11}CO_2$ gas as product. The product gas was driven out through a stainless-steel tube (0.159 cm ID (1/16 in.)) (Jahangiri et al., 2016) connected to the target body through a high-pressure valve using the N_2/O_2 target gas mixture by repeatedly pressurizing and de-pressurizing the target chamber. The product stream was led into a hot cell. In the hot cell, the $[^{11}C]CO_2$ was separated from the product stream by directing it over a nitrogen cooled Porapak N trap (Uittenbosch et al., 2018) containing porous polydivinylbenzene polymer beads, absorbing the $[^{11}C]CO_2$. The Porapak N trap was flushed with the product stream multiple times to ensure quantitative absorption of $[^{11}C]CO_2$ before disposing the exhausted target stream. The activity absorbed on the polymer was measured using a Capintec ionization chamber capable of detecting ^{11}C.

The saturation activity A_{sat} is calculated according to (Buckley et al., 2004).

$$A = A_{sat} \bullet I \bullet \left(1 - e^{-\lambda \bullet t}\right) \quad (2)$$

with A being the measured activity decay-corrected to end of bombardment (EOB), I the beam current, and λ being the decay constant of ^{11}C with a half life of 20.34 min.

3. Results & discussion

3.1. Pressure rise measurement

All irradiation results are summarized in Table 2. The pressure rise p/p_0 during irradiation is shown in Fig. 3. Both targets show an overall trend of p/p_0 rising with increasing beam current. This is expected as higher beam current correlates with increasing heat influx into the target, and according to the ideal gas law the pressure p in a closed system of volume V depends linearly on the temperature T of the system. While the target gas is not an ideal gas, it can serve as a good approximation to explain trends in the experimental results.

Overall p/p_0 is larger in the long target than in the short target. This is not expected as for a given beam current, the same amount of power is deposited in each target. The same difference in power leads to the same difference in temperature rise, which should result in the same difference in pressure rise. One explanation could be, that a greater portion of the beam in the short target is not deposited in the gas but into the target body walls due to density reduction, resulting is a lower temperature rise and consequently in a lower p/p_0. But even p/p_0 in the long target does not linearly depend on the beam current.

Also in Fig. 3 are the results from fitting the experimental data to Eq. (1). The fitting results are summarized in Table 3. It should be noted that the initial pressure p_0 is not the same for all measurements. We showed in (Jahangiri et al., 2016) that at least for our experimental conditions at

Table 2
Pressure rise and activity results from the short and long target irradiation.

Run	p/p_0 (psi)	A @ EOB (Ci)	A_{sat} (Ci/uA)
S1	1.372 ± 0.004	1.230 ± 0.031	0.0777 ± 0.0020
S2	1.366 ± 0.004	1.225 ± 0.031	0.0762 ± 0.0026
S3	1.407 ± 0.004	not measured	not measured
S4	1.407 ± 0.004	1.391 ± 0.035	0.0717 ± 0.0025
L1	1.392 ± 0.004	1.265 ± 0.021	0.0850 ± 0.0022
L2	1.502 ± 0.004	not measured	not measured
L3	1.517 ± 0.004	1.423 ± 0.036	0.0834 ± 0.0029
L4	1.536 ± 0.004	1.482 ± 0.030	0.0834 ± 0.0030

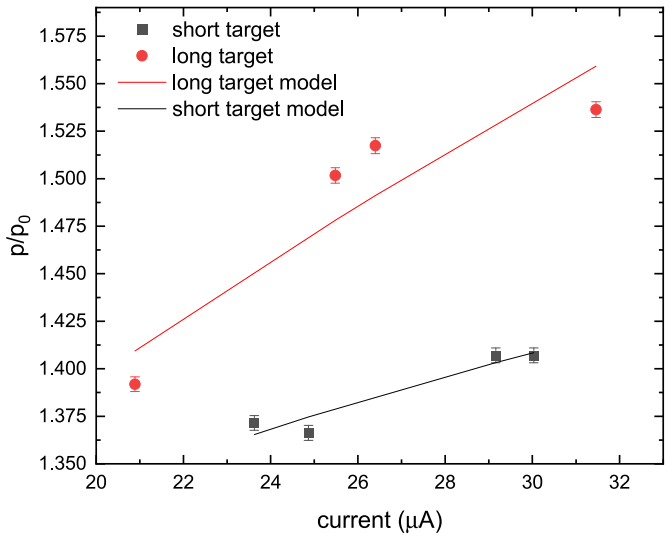

Fig. 3. Pressure rise p/p_0 for different beam currents and the results from our model (Jahangiri et al., 2016).

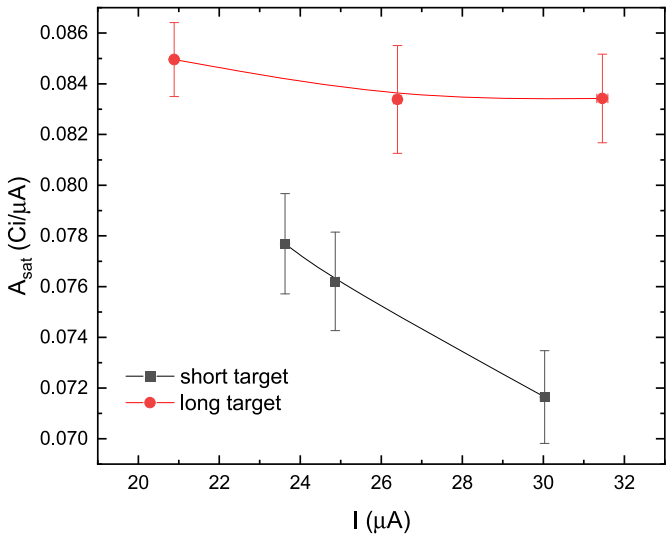

Fig. 4. Saturation activity as a function of beam current. The solid line is a spline of the data to guide the eye.

Table 3
Fitting results from model.

	$h_0\ \left(\frac{W}{m^2 \bullet K}\right)$	$h_1\ \left(\frac{W}{m^2 \bullet K}\right)$
Short target	224 ± 50	311 ± 60
Long target	131 ± 38	51 ± 47

the TR13 cyclotron, h_0 is only a weak function of p_0. On the other hand, h_1 does depend on p_0. For the short target, the initial pressure varies only by 11 psi, while for the long target it varies by 31 psi. This is reflected in the large error bar of h_1 for the long target and the larger deviation of the curve from the data points in Fig. 3.

The comparison between the two target shows that h_0 is larger in the short target than the long target. As the materials of the two targets are the same, this must be a consequence of the difference in geometry, either the larger diameter or the larger length of the long target. As density reduction may result in part of the beam being deposited into the back wall of the target, this will be less of an effect in the long target. In addition, a larger target diameter will result in less beam being lost to the target walls due to scattering. This results overall in a larger effective beam power deposition in the long target than in the short target, as already discussed above. Therefore, the short target needs to remove heat from only part of the beam power, and it appears to be more efficient.

For the short target h_1 is larger than h_0, indicating that convection is the main driver for cooling. This is not the case for the long target. For the long target h_1 is much smaller than for the short target, indicating that more cooling is removed due to convection in the short target than in the long target. One explanation could be that the smaller target has a larger temperature gradient between the center beam axis and the outer target wall, which might be more efficient in creating large convection currents. But more data with a smaller spread in initial pressure is necessary to decrease the error bar of h_1 in the data of the long target.

3.2. Yield measurement

Fig. 4 shows the saturation activity as a function of beam current. While from equation (2) it is clear that A_{sat} should not depend on I, the results from the short targets shows a clear decrease of A_{sat} for increasing I. Even for the long target it may still decrease, although this is within the error. Again, this can be explained with the effect of density reduction: for increasing I, the density reduction increases, increasing the losses of the beam to the target body wall. The lost portion of the proton beam cannot contribute to the production of ^{11}C. As in section 3.1, this effect is larger in the short target.

Fig. 5 shows the effect of the initial loading pressure p_0 on the saturation yield. The loading pressure is proportional to the amount of gas in the target. However, for a 'thick' target, where the beam is fully absorbed by the target material, an increase of target atoms in the target body overall does not increase the amount of target atoms that interact with the proton beam, and therefore does not influence the saturation activity. It is clear from Fig. 5 that in our experiment A_{sat} increases with increasing p_0 for the short target and maybe even for the long target, although the effect is within the error bars. The deviation from a flat behavior is again larger in the short target, indicating a larger density reduction effect than in the long target.

4. Conclusion

We investigated the effect of density reduction on the operating pressure and radioactive yield of Nb-body targets of different length and

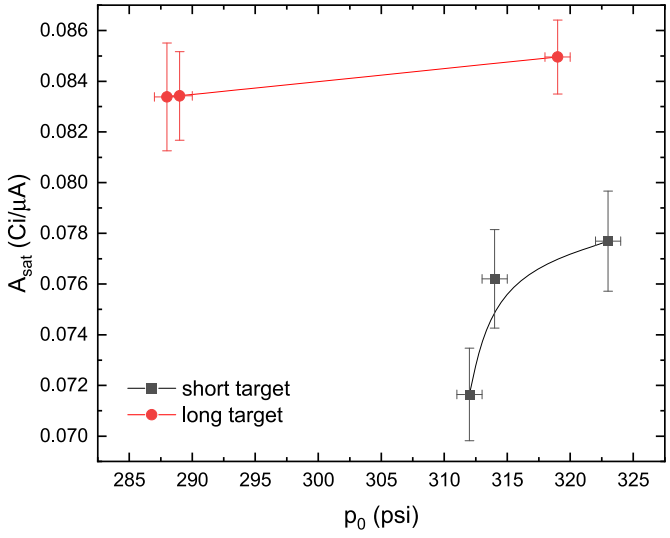

Fig. 5. Saturation activity as a function of initial pressure. The solid lines are splines of the data to guide the eyes.

diameter for the production of $[^{11}C]CO_2$. It was found that despite a nominal proton range of only ~80 mm, the 120 mm long target of 120 mm and 220 mm length showed effects of density reduction. Even the long target with a length of 220 mm may show a small density reduction effect, although the observation is within the measured error. This demonstrates that under the discussed irradiation conditions, even a target body 2.75 times the length of the proton range in a static gas may not be enough to avoid the loss of protons to the target-body walls due to thermodynamic effects and the resulting density reduction. This should be considered for any new gas-target body design.

CRediT authorship contribution statement

Lucas Mues genannt Koers: Writing – review & editing, Writing – original draft, Formal analysis. **David Prevost:** Writing – review & editing, Resources, Methodology, Investigation, Formal analysis, Data curation. **Elisabeth Paulssen:** Writing – review & editing, Supervision, Resources. **Cornelia Hoehr:** Writing – review & editing, Writing – original draft, Visualization, Supervision, Software, Resources, Project administration, Methodology, Funding acquisition, Formal analysis, Data curation, Conceptualization.

Declaration of competing interest

The authors declare that they have no known competing financial interests or personal relationships that could have appeared to influence the work reported in this paper.

Data availability

Data will be made available on request.

Acknowledgements

TRIUMF receives funding via a contribution agreement with the National Research Council of Canada (NRC). This research was funded by the National Sciences and Engineering Research Council of Canada (NSERC) via the Discovery grant program (RGPIN-2016-03972). We thank the TR13 cyclotron crew for their ongoing support in target research.

References

Buckley, K.R., Huser, J.M., Jivan, S., Chun, K.S., Ruth, T.J., 2000. ^{11}C-methane production in small volume, high pressure gas targets. Radiochim. Acta 88, 201–205.
Buckley, K.R., Jivan, S., Ruth, T.J., 2004. Improved yields for the in situ production of $[^{11}C]CH_4$ using a niobium target chamber. Nucl. Med. Biol. 31, 825–827.
Heselius, S.-J., Solin, O., 1986. A model for beam penetration in gas targets. J. Label. Compd. Radiopharm. 23, 1389–1392.
Heselius, S.-J., Lindblom, P., Solin, O., 1982. Optical studies of the influence of an intense ion beam on high- pressure gas targets. Int. J. Appl. Radiat. lsot. 33, 653–659.
IAEA. Medical isotope browser. https://www-nds.iaea.org/relnsd/isotopia/isotopia.html accessed Dec 2022.
Jahangiri, P., Zacchia, N.A., Buckley, K., Bénard, F., Schaffer, P., Martinez, D.M., Hoehr, C., 2016. An analytical approach of thermodynamic behavior in a gas target system on a medical cyclotron. Appl. Radiat. Isot. 107, 252–258.
Jahangiri, P., Martinez, D.M., Hoehr, C., 2018. Pressure rise in medical cyclotron liquid targets: transient analysis. Appl. Radiat. Isot. 136, 87–100.
Magill, J., Dreher, R., Soti, Z., 2018. Karlsruher Chart of Nuclides, tenth ed. (Nucleonica).
McDaniels, D.K., Bergqvist, I., Drake, D., Martin, J.T., 1972. Beam heating in gas targets. Nucl. Instrum. Methods Phys. Res. 99, 77–80.
Oselka, M., Gindler, J.E., Friedman, A.M., 1977. Non-linear behavior of gas targets for isotope production. Int. J. Appl. Radiat. lsot. 28, 804–805.
Robertson, L.P., White, B.L., Erdman, K.L., 1961. Beam heating effects in gas targets. Rev. Sci. Instrum. 32 (1405), 1405.
Schaffer, P., Bénard, F., Bernstein, A., Buckley, K., Celler, A., Cockburn, N., Corsaut, J., Dodd, M., Economou, C., Eriksson, T., Frontera, M., Hanemaayer, V., Hook, B., Klug, J., Kovacs, M., Prato, F.S., McDiarmid, S., Ruth, T.J., Shanks, C., Valliant, J.F., Zeisler, S., Zetterberg, U., Zavodszky, P.A., 2015. Direct production of ^{99m}Tc via ^{100}Mo(p,2n) on small medical cyclotrons. Phys. Procedia 66, 383–395.
Uittenbosch, T., Buckley, K., Ruth, T., Martinez, D.M., Hoehr, C., 2018. A forced-convection gas target for the production of $[^{11}C]CH_4$. Appl. Radiat. Isot. 140, 1–4.
Wojciechowski, P.W., Sajjad, M., Lambrecht, R.M., 1988. A semi-quantitative ap- proach to the design, analysis and operation of gas targetsystem. Int. J. Radiat. Appl. Instrum, PartA. 39, 429–436.
Zacchia, N.A., Buckley, K.R., Martinez, G.M., Ruth, T.J., Martinez, D.M., Hoehr, C., 2018. Understanding radionuclide production in gas target systems: the effect of adsorption on the target body. Phys. Med. Biol. 63, 1–26.
Ziegler, J.F., Ziegler, M.D., Biersack, J.P., 2010. SRIM – the stopping and range of ions in matter. Nucl. Instrum. Methods B 268, 1818–1823.